Available online at www.sciencedirect.com

SciVerse ScienceDirect

Ceramics International 39 (2013) 2093–2105

CERAMICS INTERNATIONAL

www.elsevier.com/locate/ceramint

Microstructure and tribological properties of pulsed electric current sintered alumina–zirconia nanocomposites with different solid lubricants

M. Erkin Cura[a,*], Seung-Ho Kim[b], Tatu Muukkonen[c], Simo Varjus[c], Antti Vaajoki[c], Outi Söderberg[a], Tomi Suhonen[c], Ulla Kanerva[c], Soo Wohn Lee[d], Simo-Pekka Hannula[a]

[a]*Department of Materials Science and Engineering, Aalto University, PO Box 16200, FI-00076 AALTO, Finland*
[b]*Industry University Cooperation Foundation, Sunmoon University, Asan 336-708, South Korea*
[c]*VTT Technical Research Center of Finland, Advanced Materials, FI-02044 VTT, Finland*
[d]*Department of Environment Engineering, Sunmoon University, Asan 336-708, South Korea*

Received 11 July 2012; received in revised form 21 August 2012; accepted 23 August 2012
Available online 30 August 2012

Abstract

Dense Al_2O_3-15 wt% (ZrO_2-3 mol%Y_2O_3) nanocomposites modified with 3 wt% of self-lubricating component (CaF_2, BaF_2, MoS_2, WS_2, h-BN, or graphite) were consolidated by pulsed electric current sintering. Their microstructure as well as mechanical and tribological properties were evaluated. During consolidation composition of the self-lubricating components was conserved except for BaF_2, which partially melted. The Al_2O_3/ZrO_2(3 mol%Y_2O_3) matrix showed hardness of 20.35 GPa and Young's modulus of 320 GPa determined by Vickers indentation. All solid lubricant additives led to a decrease in hardness of the composite. Solid lubricant additives lowered the coefficient of friction (CoF) against alumina at room temperature. In pin-on-disc tests CoF of 0.38–0.42 was measured for all the materials against alumina ball. The lowest CoF of 0.043 was measured for Al_2O_3/ZrO_2(3 mol%Y_2O_3)/CaF_2 in the scratch test against diamond stylus while the matrix material showed lower friction than other materials. The measured wear rates were in the order of 10^{-12} for Al_2O_3/ZrO_2(3 mol%Y_2O_3)/CaF_2, Al_2O_3/ZrO_2(3 mol%Y_2O_3)/MoS_2, and Al_2O_3/ZrO_2(3 mol%Y_2O_3)/WS_2.

Keywords: Pulsed electric current sintering; B. Nanocomposites; C. Mechanical properties; D. Al_2O_3

1. Introduction

In demanding environments where high temperature, corrosive medium, or very high loads are dominant, structural ceramics exhibit superior properties compared to metals [1]. They retain high hardness and chemical stability, and their strength is good. However, there are limitations especially because of their low toughness [2]. It is possible to improve their ductility by modifying the deformation mechanisms, for example, by reducing the grain size of ceramics into the nanometer scale [3]. In order to obtain fully dense nanostructured ceramics novel processing methods have been employed and extensively studied in the last decade [3–7]. Furthermore, the strength and fracture toughness can be improved by dispersing nanosized inclusions within the ceramic matrix [3]. Another route of toughening of alumina matrix is based on the addition of tetragonal zirconia (t-ZrO_2) stabilized with Y_2O_3 (Y-TZP), which goes under superplastic deformation [8–11]. In multiphase ceramics t-ZrO_2 improves toughness and thermal stability because of the segregation of nanosized additive particles in the grain boundaries [12–14]. These nanocomposites show also reduced grain growth, which enhances the strain hardening at high temperature [8,12]. Alumina can readily be used in such multiphase nanocomposite as it is relatively inexpensive material with exceptional hardness and thermal properties. When it contains Y-TZP, it exhibits good room temperature toughness and wear resistance [1,15–18]. Furthermore,

*Corresponding author. Tel.: +358 9 47022683; fax: +358 9 47022677.
E-mail address: erkin.cura@aalto.fi (M. Erkin Cura).

0272-8842/$ - see front matter © 2012 Elsevier Ltd and Techna Group S.r.l. All rights reserved.
http://dx.doi.org/10.1016/j.ceramint.2012.08.065

it is also favourable for elevated temperature applications, where sliding or reciprocal movement is of interest (bearings of turbine rotors, vane bushings, rolling bearings etc.).

Typically, in dry sliding conditions, the wear rate and CoF for ceramic materials at room temperature are approximately $\sim 10^{-6}\,mm^3/Nm$ and 0.4, respectively [1,19]. These values are not low enough for reducing energy losses in the moving parts. In general, the low friction materials should exhibit CoF below 0.2 in order to minimize the heating and thermal gradients and to avoid fatigue wear. Although Y-TZP addition improves toughness, wear resistance and hot hardness, alumina–zirconia composites have relatively high wear rates and CoF at high temperature [20,21]. Above $\sim$350 °C, hydrocarbon based lubricants are not applicable, and the dry friction takes place. Therefore, solid lubricants are used for reducing CoF [22–25]. These include soft metals, metal oxides, alkaline earth fluorides, lamellar solids, barite structures, etc [26,27]. Solid lubricants are beneficial from a tribology point of view; however, they impair the mechanical properties, strength and hardness. If they are added in high volume fractions, even though the friction may be reduced significantly, the wear of the material can become severe [1]. It has been shown that solid lubricants in plasma sprayed ceramic coatings improve both the wear resistance and friction properties [28–30]. More control on the microstructure and chemical composition of the material is gained with the powder metallurgical (PM) methods.

There are many different methods for manufacturing of nanosized powders and consolidating them. The difficulty is to achieve dense ceramics with nanosized grains. Solid state or liquid phase sintering processes provide almost fully dense materials, while pressure assisted sintering promotes mechanical properties, too. In pressureless sintering of alumina matrix composites processing temperature may be as high as $\sim$1727 °C and the dwell time is hours [31,32]. In such a process, it is not possible to retain a nanosized microstructure, since the grain growth is unavoidable. Lowering the sintering temperature and duration is possible by means of rapid heating and use of pressure. Among many methods pulsed electric current sintering (PECS), also known as spark plasma sintering (SPS) or field assisted sintering technique (FAST), has drawn particular attention [7,28,33,34]. In PECS the measured sintering temperature is usually 100–200 °C lower and the dwell time is from 0 to 20 min instead of hours in comparison with conventional methods [6,34]. The pulsed current is applied through the mould/powder system. If the powder is conductive, it is heated by its specific resistance; when powder is an insulator, the heating is conductive and occurs by the rapidly increasing temperature of the mould [35]. The heating rates can be even a thousand degrees per minute, though usually it is kept around 50–200 °C/min. Rapid heating, pressure, low sintering temperature, and short dwell time are all in favour of retaining the nanosized microstructure [36].

In the present study, ceramic nanocomposites are consolidated by PECS and their microstructure, mechanical, friction, and wear properties are studied. Influence of calcium fluoride (CaF_2), barium fluoride (BaF_2), molybdenum sulphide (MoS_2), tungsten sulphide (WS_2), hexagonal boron nitride (h-BN), or graphite on the properties of Al_2O_3+15 wt% (ZrO_2+3 mol% Y_2O_3) nanocomposite matrix is evaluated. Previously, it has been shown that the same ceramic matrix material, with 1 wt% addition of CaF_2, h-BN, or graphite exhibits friction coefficient below 0.3 in the ball-on-plate wear test at room temperature [37]. In the present work, the amount of the additive is increased to 3 wt% and with other solid lubricants they are tested at room temperature. Presence of solid lubricants usually degrades the mechanical strength of the matrix material and sometimes poor mechanical properties are more significant than good friction and wear properties. Accordingly, effect of the additives on hardness, densification and microstructure of the composites is investigated.

2. Experimental

2.1. Powder preparation and characterization

A self-lubricating component either CaF_2, BaF_2, MoS_2, WS_2, h-BN, or graphite amounting of 3 wt% was added to the Al_2O_3+15 wt% ZrO_2 nanocomposite. Later in the text the matrix is also referred as AZ, while the additives are abbreviated as CF, BF, MS, WS, BN, and GR corresponding to the order above.

At first the alpha alumina powder (AKP-53, Sumitomo Chem. Ltd. Co. Japan) with the average particle size of 290 nm was mixed in planetary mill for 12 h with the yttria stabilized zirconia powder (TZ-3YE, Tosoh Corp. Japan) having the average particle size of 27 nm. CaF_2, BaF_2, MoS_2, WS_2, and h-BN powders (all from High Purity Chemicals, Japan) had average particle sizes of 1–10, 1–5, 0.5–5, 1–10, and 2–5 μm, respectively. The graphite powder (N&A Materials Inc., USA) had an average particle size of 450 nm. The AZ and additive powders were mixed in ethanol for 24 h and then dried in rotary evaporator and in oven at 80 °C for 24 h. The particle size distribution of the powders (Fig. 1) was established by the laser method (Lecotrac LT100) in water after ultrasonic mixing for 60 s. Powder morphology and the chemical analysis of the particles were examined with scanning electron microscope (Hitachi S-4700 equipped with INCA EDS), and their crystallographic structure was evaluated applying θ–2θ scan by the Philips PW 3830 powder diffractometer (Cu K_α radiation, 2θ of 10–90°, scan speed of 0.02°/s).

2.2. Pulsed electric current sintering

Powders were consolidated with pulsed electric current sintering (PECS) by using a FCT HP D 25-2 unit. The powders were compacted in cylindrical graphite moulds

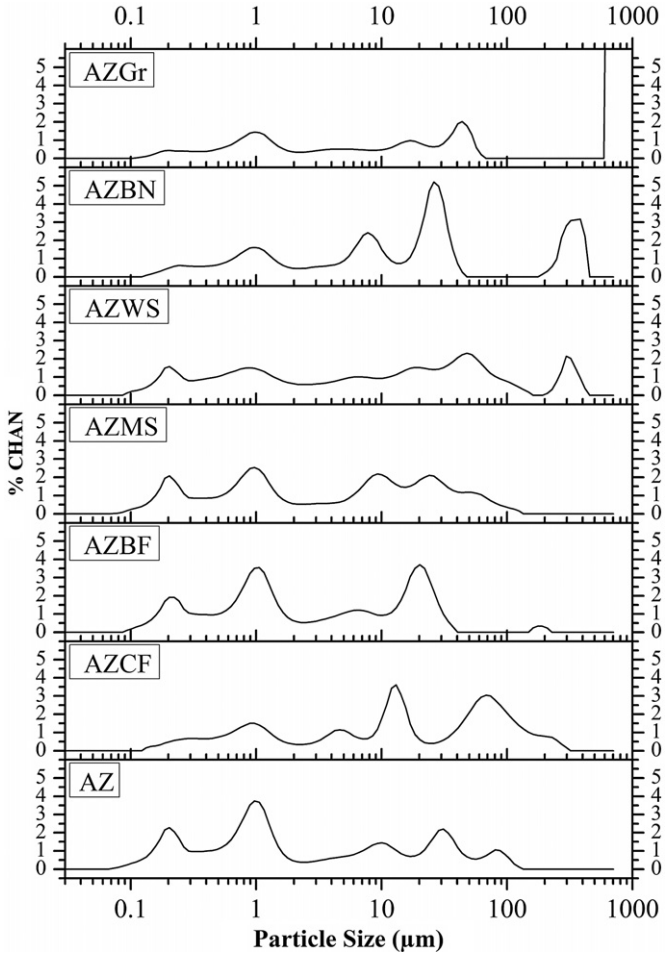

Fig. 1. Particle size distributions of the powders used in the experiments.

having an inner diameter of 20.8 or 40.8 mm. Graphite foils with a thickness of 0.4 mm were placed in between the powder and the graphite surfaces in order to prevent any reaction and to increase the contact area between them. Graphite felt was used for insulation in order to keep the heat within the mould and to avoid thermal gradients [38]. In the applied equipment configuration, the processing temperature was measured by a pyrometer through the upper punch hole from the thin graphite wall surface at 5 mm distance from the powder. The pyrometer had response time of 2 ms and accuracy of 0.3% of measured value in °C. Control of the processing temperature as well as the steps of sintering cycle was carried out based on the pyrometer readings.

Samples with diameters of 20 and 40 mm were consolidated for microstructural and mechanical characterization and for the tribology tests, respectively. For each disc shaped sample with diameter of 20 mm and height of 5 mm, approximately 6.5 g of powder was used. Samples with 40 mm diameter and height of 5 mm needed approximately 27 g of powder. For both dimensions the powders were sintered at 1300 °C for 5 min. Uniaxial pressure of 50 MPa was applied at room temperature, kept on until the end of sintering stage, and gradually removed during cooling. The D.C. current was applied to the graphite mould via steel electrodes in pulses, which were 10 ms long and followed by a 5 ms pause. Sintering was carried in a vacuum of about 6 Pa. The heating rate was 100 °C/min in the temperature region of 400–1275 °C. In the final 0.5 min of the heating stage heating rate was decreased to 50 °C/min in order to minimize the over shooting in the temperature to 3 °C. Cooling from the processing temperature to 60 °C took place in 6 min, which corresponds to an average cooling rate of about 200 °C/min. In Fig. 2a, the piston travel speeds (p.t.s.) recorded together with the temperature during the process are given for all the studied materials when compacting samples with a diameter of 20 mm. During densification, the porosity is reduced and eventually eliminated. The speed of the piston movement in macro scale is related to the densification of the compact and can thus yield information about the progress of densification and shrinkage of the powders.

The displacement of the moving piston corresponds to the change in the height of the powder ($\Delta L < 0$), which is the difference between instantaneous height (L) and initial

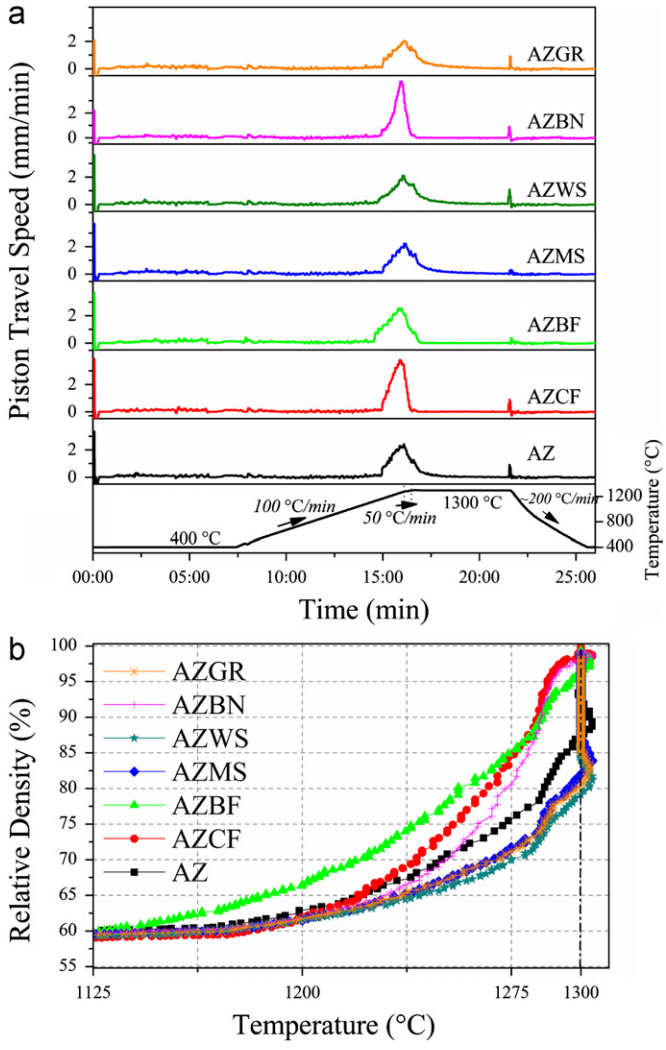

Fig. 2. (a) Evolution of temperature and the piston travel speed during the PECS process. (b) The instantaneous change in relative density between 1125 and 1300 °C including the dwell time.

height (L_0). The shrinkage in the powder height was used to calculate the momentary relative density of the sample by using the relation between height and relative density of the sample in course of the sintering by $D=(L_f/L)D_f$ [39]. In the formula D is the instantaneous relative density, L_f is the final height of the sample, L is the instantaneous height of the powder bed and D_f is the final relative density. The pressure was applied at room temperature before the heating was started. By the start of the heating cycle the samples had reached their highest green densities (under the applied pressure). The change of relative density with the increasing temperature for each material is depicted in Fig. 2b. Clear changes in the relative densities of the materials occur up to the sintering temperature and the dwell period. The sintering temperature of 1300 °C is marked and the peaks exceeding this mark on the y-axis values represent the overshooting in the sintering temperature. The linear increase at the sintering temperature, which was observed for some of the composites, represents densification that took place in the dwell period. The raw data used for constructing Fig. 2 were corrected for thermal expansion taking place in the equipment, which was determined by conducting a dummy test using only the graphite mould and foils.

2.3. Characterization of the consolidated materials

Surfaces of the compacts were cleaned from graphite foils with sandblasting. Some grinding was conducted to eliminate the porosity at the very surface caused by the graphite foil. Densities of the samples were measured by applying the Archimedes method in deionised water. For the indentation studies, SEM examinations and scratch tests, cross sectional samples ($20\times4\times2$ mm^3) were cut from the compacts by a diamond saw, and mounted in epoxy buttons, while XRD studies were made on pieces of the compact. All samples were ground with diamond discs (120–1200 grits) and polished with diamond paste (6, 3, and 1 μm). A final polishing was made by colloidal silica (0.06 μm, pH 9.8) for the SEM studies. SEM/EDS and XRD studies of the sintered materials were carried out with same equipment that was used for the powders. Grain size measurements were conducted by using image analysis on several secondary electron images of thermally etched samples [40,41].

Hardness and ductility were studied by HV1 microhardness measurements using the Zwick/Roell ZHU 0.2 apparatus, which allows also recording of the indentation depth and applied force. The scratch test was carried out with a CSM Micro-Combi Tester with a Rockwell diamond tip ($r=200$ μm) under an increasing load from 1 to 30 N, by a loading rate of 50 N/min and stylus speed of 10 mm/min. The coefficient of friction was obtained almost at the end of the test when the load was approximately 27 N in 50% humidity.

Pin-on-disk tests with the samples of 40 mm in diameter were carried out for measuring wear rates and friction coefficients of the materials against alumina. Test specimen surfaces were prepared by the same steps applied for the samples used in microstructure characterization and cleaned by acetone in an ultrasonic cleaner. The surface roughness (R_a) of the materials were 0.1, 0.02, 0.03, 0.02, 0.06, 0.04, and 0.03 μm for AZ, AZCF, AZBF, AZMS, AZWS, AZBN, and AZGR, respectively, measured with the Veeco Dektak 6M stylus profilometer. Three pin-on-disk tests were performed for each specimen at room temperature in 50% humidity, with an alumina ball (diameter: 10 mm, R_a: 0.2 μm) by applying a load of 10 N for sliding distance of 1000 m at a sliding speed of 0.5 m/s. Wear track profiles were analyzed by the same profilometer using a tip with a diameter of 12.5 μm and applying a load of 1 mg. The wear rates of the specimens were calculated dividing wear volume, which were derived from the 2D profiles, by the normal load and sliding distance. Wear rates and the average CoFs were used for evaluation of the effect of solid lubricants on tribological properties of the materials. The tests were followed by a study of the wear tracks by SEM.

3. Results

3.1. Powder characteristics and densification

In the powders nanosized ZrO_2 particles were distributed homogeneously among the submicron sized Al_2O_3

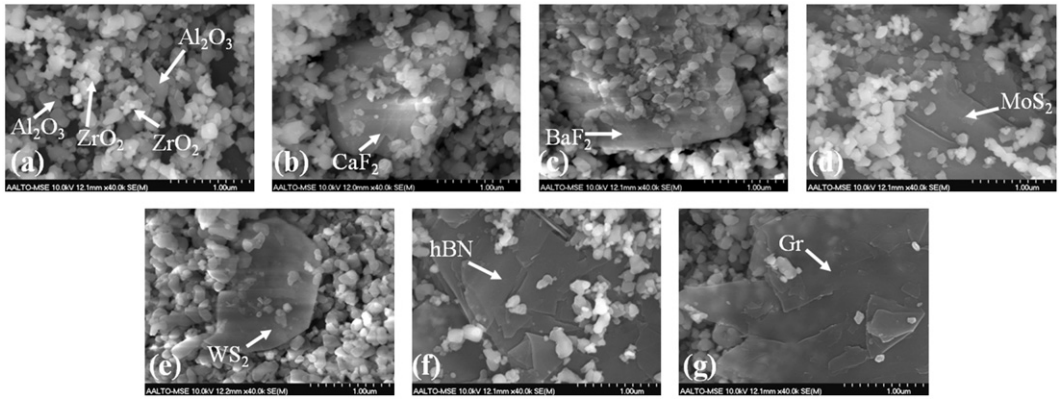

Fig. 3. SEM micrographs of (a) AZ, (b) AZCF, (c) AZBF, (d) AZMS, (e) AZWS, (f) AZBN and (g) AZGR powders. The single large particles on each image indicate the additive particle. The scale on the images is 1 μm.

particles (Fig. 3a). Alumina particles had an angular shape while zirconia particles were more rounded. The laser diffraction measurements, which show much higher d_{90} values than for d_{10} fraction (Fig. 1), indicate marked size difference of the matrix and low friction additive powders. Fig. 3b–g illustrates this difference between the low-friction additive particles and the alumina and zirconia particles. Furthermore, the particle sizes after the composite powder preparation were larger than the original particles of the raw material powders due to agglomeration, which was more severe in the presence of the low friction additives. This can be attributed to adhering and embedding of harder alumina and zirconia particles to softer and lamellar shaped additive particles.

The applied sintering parameters for PECS were similar to earlier studies [36,37]. The sintering temperature, pressure and duration were kept the same for all the powders in order to acquire similar microstructures with the ceramic matrix. The measured and relative densities of the compacts are given in Table 1. Here, the theoretical density is calculated based on the amounts and densities of the different components in the powder. The densification behaviour of the composites as evaluated from the change in the sample height and the relative density accordingly and the displacement rate of the moving electrode, i.e., upper piston's travel speed, is presented in Fig. 2a and b. Bare AZ was consolidated almost to its full density, although only during the last 1 min of dwell period there was no piston movement observed. In case of AZCF, AZBF, and AZBN the densification was also nearly complete, but took place more rapidly. Relative density of about 99% was achieved already before the sintering temperature was reached and the p.t.s. was zero almost immediately after reaching this temperature. AZBF had a more rapid densification starting at about 1120 °C – at a much lower temperature as compared to other composites – and only at about 1280 °C AZCF and AZBN surpassed AZBF in terms of relative density. The applied sintering parameters were also adequate for achieving full densification of AZMS, AZGR, and AZWS, for which relative density of about 80–85% was obtained when the sintering temperature was reached and final stage of densification took place during the dwell period. The piston movement was continuous during the dwell time at the sintering temperature resulting in the density close to 99%. Here, it is noteworthy that the decomposition temperatures of MoS_2 and WS_2 are below the processing temperature of 1300 °C, i.e., 1185 and 1250 °C, respectively.

3.2. Microstructure evaluation

The phase structure of the sintered compacts were studied by XRD and compared to that of the starting powders (Fig. 4). In all the powder mixtures and consolidated compacts alumina was in the alpha form, which is the most stable Al_2O_3 phase [43]. In the powders monoclinic ZrO_2 was observed, but in the compacts all the zirconia exhibited tetragonal structure (Fig. 5). MoS_2, WS_2, and graphite were in hexagonal form before and after sintering. CaF_2 and BaF_2 existed in the respective powders and compacts in cubic phase. Only additive that could not be detected clearly by XRD was the hexagonal boron nitride. This is most probably due to the removal of the h-BN from the surface during the specimen preparation as the adhesion of h-BN to the matrix was very poor. XRD studies did not reveal any amorphous (glassy) phase in powders or compacts.

The morphology and distribution of various phases in the cross sections of the compacts were studied by SEM. The backscattered electron mode (BSE) revealed clearly the regions with different densities, while the different phases in the structures were confirmed with the EDS element mapping (e.g., Fig. 5).

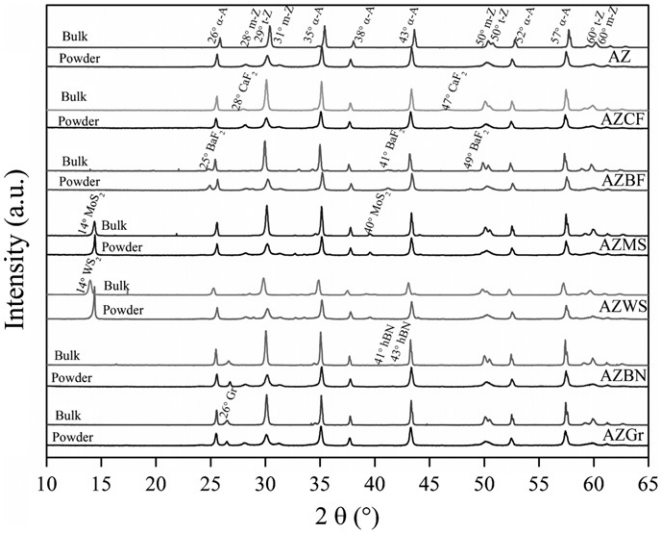

Fig. 4. XRD patterns of the starting powders and sintered compacts.

Table 1
Density of AZ and its composites.

		AZ	AZCF	AZBF	AZMS	AZWS	AZBN	AZGR
Density (g/cm^3)	Measured	4.18	4.14	4.17	4.16	4.12	4.04	4.02
	Theoretical[a]	4.19	4.15	4.21	4.21	4.25	4.07	4.08
	Relative (%)	99.7	99.9	99.2	98.9	96.9	99.4	98.5

[a]Calculated densities of the composites by using the theoretical densities of the components [42].

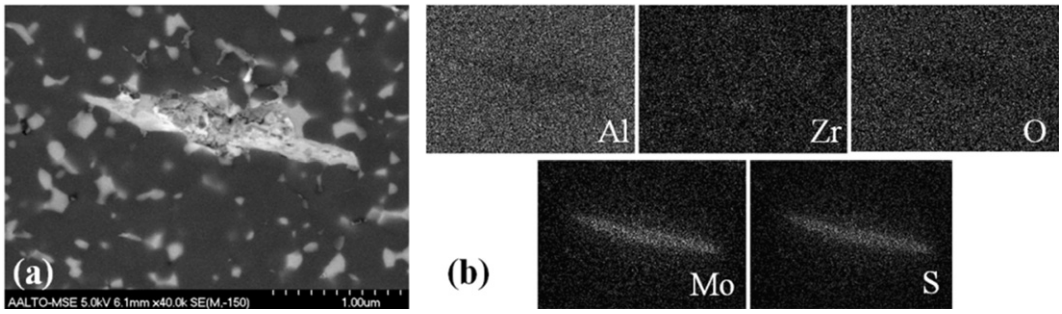

Fig. 5. (a) SEM-BSE image of a MoS_2 grain and (b) element mapping from the same region.

Throughout the matrix of all the studied composites the ZrO_2 grains were observed in inter- and intragranular locations. In Fig. 6a the dark grains are of Al_2O_3 and light grains are of ZrO_2. In addition to the nanosized grains zirconia existed also within larger regions formed from the agglomerated powder in sintering (Fig. 6b). The measured grain sizes of Al_2O_3 and ZrO_2 grains in AZ were about 410 and 105 nm, respectively. It seems that in the composites their grain sizes varied to some extent. Grain size of alumina was in the range of 390–525 nm while that of zirconia was varied from 94 to 160 nm for all the composite materials which were very similar in their microstructure (Table 2).

In all composites the soft and low-strength solid lubricant additives were located intergranularily. The CaF_2 addition seemed to have more integrity with the AZ matrix, but it was easily removed and smeared under load, which was beneficial in scratch tests. In AZMS and AZWS additives had mostly needle-like shape with width of about 200–500 nm and length of about 1–15 μm, respectively (Figs. 5 and 7a and b). Especially, in AZWS the additive particles with planar morphology had formed a distinct layered lamella structure (Fig. 7b, light grey area) during the axial compression applied in the PECS process. There are particles as big as 10 μm in length due to large agglomerates in the starting powders, along with much smaller grains with similar shape (Fig. 7a). Boron nitride appeared in different shapes and sizes embedded in the AZ matrix with clearly separated regions, which may be correlated to its low adhesion to the matrix resulting in the pop-outs of the h-BN phase during the specimen preparation (Fig. 7c and d). Again the planar shaped powders had transformed in processing to needle shaped grains with width of about 0.1–2 μm and length of about 0.5–15 μm. Fig.7e and f show the structure of AZGR. The graphite regions varied in shape and size, some of them being as large as 10 μm in width. The flake structure inside graphite consisted of thin and sharp grains.

Unlike the other additives, BaF_2 had locally melted and was seen as large BaF_2 rich regions in the structure (Fig. 8a). These regions could be even 40 μm in diameter. Within these areas grains of ZrO_2 and Al_2O_3 were observed. However, the morphology of the embedded alumina and zirconia grains was more rounded indicating their partial dissolution to the BaF_2 rich phase (Fig. 8b).

3.3. Mechanical properties

In Table 2 hardness, Young's modulus and grain size of AZ are given together with values from some earlier studies in literature on pure alumina and alumina/zirconia composites with alumina or zirconia matrix and consolidated by PECS technique and in Table 3 mechanical properties, CoF and the wear rates of AZ and its composites are summarized.

Hardness and Young's modulus in Table 3 were determined based on the indentation tests (Fig. 9). In Fig. 9 only selected measurements of each material are shown. The indentation tests showed that the hardness of the nanocomposite decreased as soft solid lubricant additives were added to the alumina–zirconia matrix.

3.4. Friction and wear properties

The friction coefficients were measured using pin-on-disc and scratch tests. Coefficients of friction (CoF) obtained in the pin-on-disc studies with the alumina ball did not give marked differences between the different materials at room temperature (Table 2). The coefficient of friction for AZ was 0.50 at RT and decreased below 0.40 in presence of different low-friction additives. The lowest CoF values of 0.39 and 0.38 were measured for AZMS and AZGR, respectively. AZBN had the highest CoF of 0.42 among the modified compositions.

The wear rates of the composites were in the order of $10^{-10}-10^{-13}$ $mm^3/N\,m$, which is significantly low for the applied test conditions (Table 2). AZ exhibited a wear rate of 5.6×10^{-10} $mm^3/N\,m$. Wear rates of AZBN and AZGR were 1.4×10^{-11} and 5.5×10^{-13} $mm^3/N\,m$; where AZCF, AZBF, AZMS, and AZWS showed wear rates of 2.3×10^{-12}, 7.6×10^{-12}, 9.3×10^{-12}, and 1.7×10^{-12} $mm^3/N\,m$, respectively. The correlation between the amount of wear and material properties is difficult to establish due to significantly low wear values. Similar features were observed on the worn surfaces of the materials. In general, except for AZ, the wear tracks as well as wear related damage on the surfaces were hard to observe. However, it was noticed that

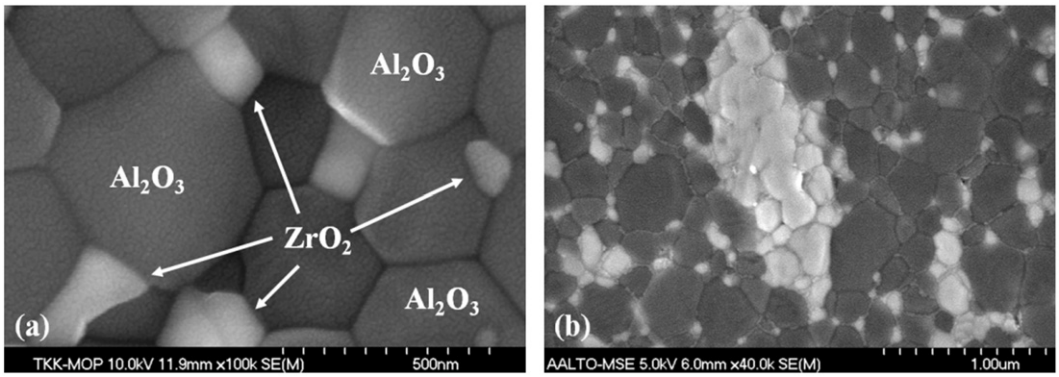

Fig. 6. Microstructure of AZ after thermal etching. (a) Light ZrO_2 grains and dark Al_2O_3 grains. (b) Large ZrO_2 cluster formed in sintering from the agglomerated particles.

Table 2
Comparison of hardness, Young's modulus and grains size with literature values.

Material	Hardness (GPa)	Young's modulus, E (GPa)	Grain size (μm)		Powder particle size (μm)	
			Al_2O_3	ZrO_2	Al_2O_3	ZrO_2
Al_2O_3+15 wt% ZrO_2 (3 mol% Y_2O_3)—this study	20.35 ± 0.50	322 ± 10	0.410	0.105	0.290	0.027
Al_2O_3+5 vol% ZrO_2 (3 mol% Y_2O_3) [2]	22.29 ± 0.51		~0.2		0.2	0.06–0.100
α-Al_2O_3+20 vol% ZrO_2 [3]	15.2		0.349		0.032	0.9
ZrO_2 (3 mol% Y_2O_3)+20 wt% Al_2O_3 [8]	15.8		0.5–1.5	0.020–0.1		0.057
ZrO_2 (4.5 mol% Y_2O_3) [21]	12.36					
ZrO_2 (3 mol% Y_2O_3) [22]	14.22					
ZrO_2 (3 mol% Y_2O_3)+20 wt% Al_2O_3 [22]	16.87		< 1		0.026	0.026
Al_2O_3+ZrO_2 (3 mol% Y_2O_3) [44]		392	0.8		0.210	0.230
Al_2O_3 [44]		407	1.9		0.210	
α-Al_2O_3[45]	20.0 ± 0.50	390	2		0.2	
α-Al_2O_3[46]	20.3 ± 0.25		0.349		0.050	

solid lubricants were not spread well enough to form a continuous tribo film due to their low amount, but some wear grooves were observed in some of the modified materials (Fig. 10). The wear mechanism was controlled by brittle fracture and pull outs of matrix grains. It was observed in AZ more significantly (Fig. 10a) In AZCF and AZMS some localized brittle fractures occurred due to stress induced intergranular cracks on the worn surfaces (Fig. 10b and c). The surface of AZWS was smoother than AZ and other modified materials. Only minor surface scratching was observed (Fig. 10d). AZGR had the lowest wear rate, which had large flake like regions of graphite on the worn surface.

CoF of the compacts against diamond stylus were determined from the dynamic loading (1–30 N) scratch test results at the applied load of 27 N (Fig. 11). Values given in Table 3 are the average of three independent tests. AZ had relatively low CoF among all the materials regards to its high density, fine microstructure, and smooth surface. It is noteworthy that even though the composites had high densities, the soft solid lubricant fragments were severely damaged during sample preparation. Shallower regions and cracks along the grain boundaries could be observed. The lowest CoF was obtained with AZCF. This resulted from CaF_2 phase smearing onto the surface during tip/surface interaction (Fig. 12). The material removal from the CaF_2 grains was more severe for the already damaged grains

4. Discussion

It has been shown that it is possible to fully densify alumina–zirconia composites with 5 and 10 vol% Y-TZP by PECS at 1400 °C in 2 min [2] and at 1150 °C in 3 min [3], respectively. The sintering parameters (1300 °C, 5 min, 50 MPa) applied in the present study were adequate also for densification of the alumina–zirconia-based composites in most cases. Although the decomposition temperatures of MoS_2 and WS_2, i.e., 1185 and 1250 °C, respectively, are below the processing temperature of 1300 °C, no decomposition of these self-lubricating additions was observed. The XRD study confirmed the existence of MoS_2 and WS_2 in the compacts. The short processing time and applied pressure obviously prevented their full decomposition. When approaching to the processing temperature, the p.t.s. of AZ started to increase at 1180 °C, while the respective value for AZMS was 1156 °C and for AZWS 1137 °C. In the PECS process the measured temperature is usually somewhat lower than the actual

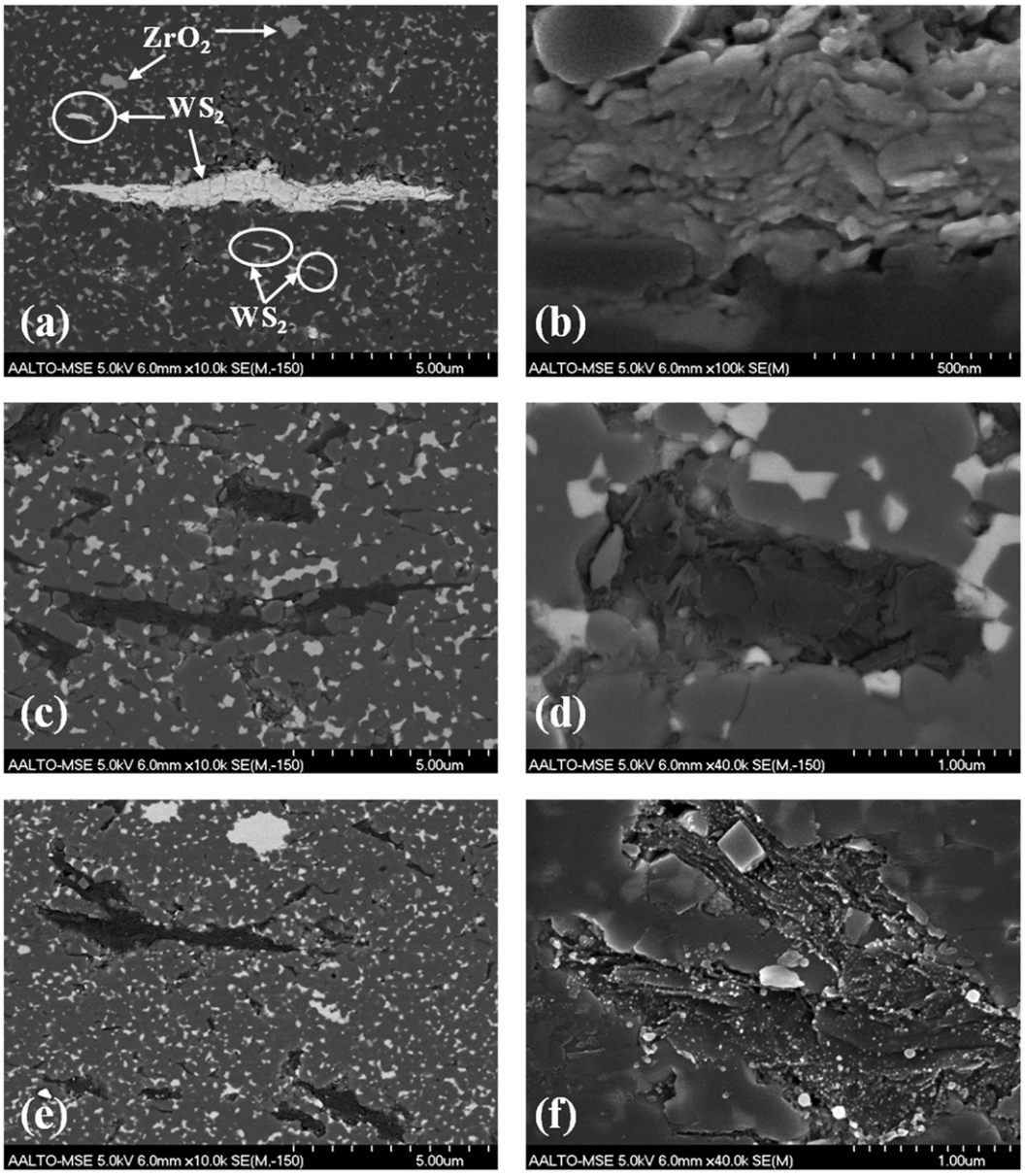

Fig. 7. (a) SEM-BSE image showing a large WS_2 region (large white area), smaller WS_2 grains (white) and ZrO_2 (light grey) in the AZWS composite. (b) Enlarged WS_2 grain, arranged in a layered, lamellar structure, which is to some extent accommodated with the matrix. (c) Large dark regions of h-BN in AZBN consisting of (d) flakes of h-BN weakly detached to the matrix. (e) In AZGR graphite appeared as large dark regions, where (f) it consisted of randomly oriented flakes.

temperature of the material and in some cases melting of the materials starts clearly below the melting point most probably due to the temperature measurement methodology and formation of thermal gradients within the material/mould structure [37,47]. This may be the reason, why the p.t.s. started to increase with AZCF at 1160 °C and with AZBF already at 1117 °C. Also, the melting temperatures of the added fluorides are rather close to the processing temperature, 1418 °C for CaF_2 and 1368 °C for BaF_2. The morphology of the embedded alumina and zirconia grains in BaF_2 region indicates their partial dissolution in the BaF_2 phase. This may explain the increase in the piston travel speed already at 1117 °C, at a clearly lower temperature than for the other materials, indicating melting of BaF_2 during the processing. Phase transformations are not relevant when considering h-BN or graphite both sublimating fairly above the processing temperature.

In the sintered AZ matrix and composites phase transformation of zirconia from monoclinic to tetragonal crystalline structure was observed. Typically it takes place at 950 °C on cooling and is reversible at 1150 °C on heating [48,49]. Zirconia was in tetragonal form after the sintering in all composites, which is also possible in some cases. Rapid cooling yields formation of a different tetragonal phase that does not directly transform into monoclinic form [48]. In addition, when oxygen vacancies are present in the structure formation of

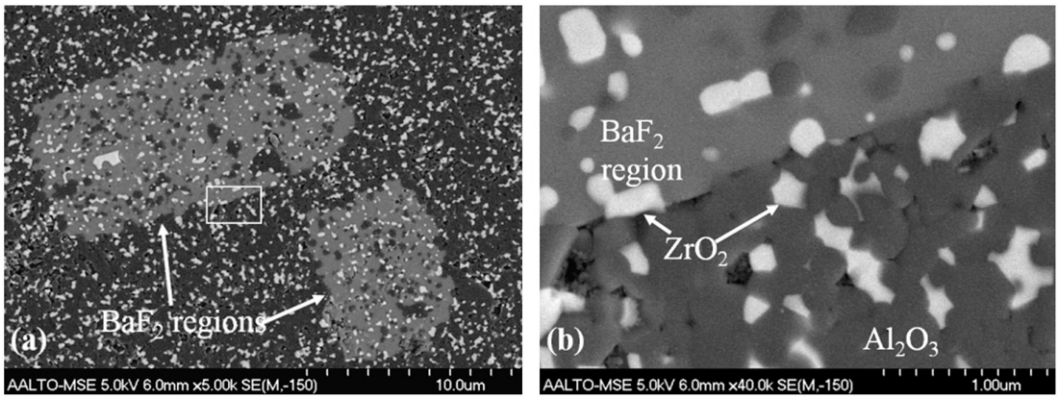

Fig. 8. SEM-BSE images for (a) BaF_2 rich regions in the AZBF composite matrix and (b) matrix/BaF_2 boundary with dispersed ZrO_2 and Al_2O_3 particles in both areas at a higher magnification.

Table 3
Mechanical properties, CoF and the wear rates of AZ and its composites.

		AZ	AZCF	AZBF	AZMS	AZWS	AZBN	AZGr
Hardness (GPa)		20.35 ± 0.5	18.13 ± 0.8	16.92 ± 0.8	18.79 ± 0.8	17.94 ± 0.4	15.80 ± 0.6	15.54 ± 0.5
Young's modulus, *E* (GPa)		322 ± 10	319 ± 28	323 ± 9	334 ± 10	287 ± 13	313 ± 8	298 ± 8
CoF (scratch test, at 27 N, diamond)		0.068 ± 0.0018	0.043 ± 0.0004	0.082 ± 0.0031	0.086 ± 0.0016	0.093 ± 0.0018	0.086 ± 0.0027	0.121 ± 0.0031
CoF (pin-on-disc, alumina ball)		0.50 ± 0.111	0.40 ± 0.006	0.41 ± 0.034	0.39 ± 0.018	0.40 ± 0.009	0.42 ± 0.016	0.38 ± 0.004
Wear rate (mm^3/N m)		5.6 E−10	2.3 E−12	7.6 E−12	9.3 E−12	1.7 E−12	1.4 E−11	5.5 E−13
Grain size (nm)	**Al_2O_3**	410	470	408	406	393	525	394
	ZrO_2	105	156	156	94	120	128	107

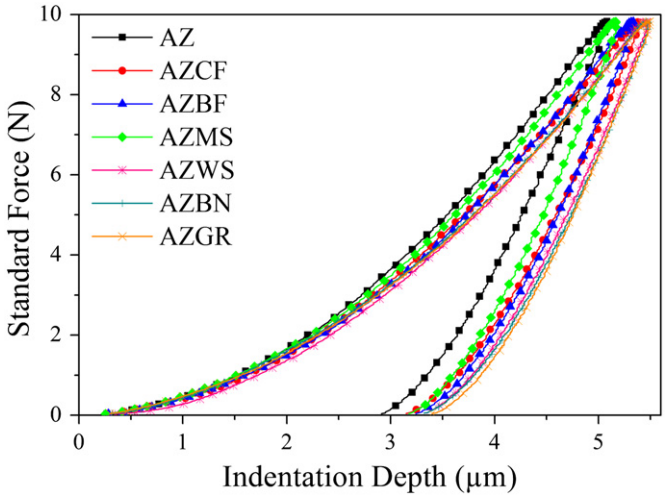

Fig. 9. Representative indentation curves of the nanocomposites (out of five for each material).

tetragonal phase requires lower energy than monoclinic phase, which destabilizes the first [50]. In sintering of AZ and composites by PECS, combination of fast heating and cooling together with reducing environment in the process zone (graphite moulds) influenced the transformation kinetics of zirconia.

The hardness of AZ is higher than pure zirconia and zirconia matrix composites with alumina additives because of the hard alumina matrix. In addition, hardness of AZ was equal or higher than PECS consolidated conventional α-Al_2O_3. Hardness of 20.35 ± 0.5 GPa was measured for AZ, while Huang et al. and Zhan et al. reported hardness of 20.5 ± 0.5 and 20.3 ± 0.25 GPa for pure alumina, respectively [45,46]. The hardness of AZ was higher than that of alumina composite with 20 wt% Y-TZP [3], but lower than that with 5 wt% Y-TZP [2]. The hardness of composites with zirconia matrix and alumina additives are between 15 and 17 GPa and clearly lower than that of AZ [8,21,22]. Zhan et al. [46] reported grain size of 349 nm with a grain size growth factor (GF) of almost 7, while 410 nm and 1.4 were obtained in the present study for AZ, respectively. The GF for alumina (pure or in a composite) varies from 3.8 to 38.5 according to [2,3,8,22,44–46]. This difference indicates profoundly suppressed grain growth in present study. Also Trombini et al. [2] reported almost no grain growth for alumina in $Al_2O_3 + 5$ vol% ZrO_2 (3 mol% Y_2O_3) composite which was consolidated at 1300 °C for 2 min and had a relative density of 99.5%. Effect of grain size on the hardness appears to be in accordance with the grain size–hardness relationship. Hardness of AZ is slightly lower when compared to $Al_2O_3 + 5$ vol% ZrO_2 (3 mol% Y_2O_3) composite of Trombini et al. [2] and higher when compared to $Al_2O_3 + 20$ vol% ZrO_2 (3 mol% Y_2O_3) composite of Zhan et al. [3]. This is probably the result of higher content of zirconia, which has lower hardness than

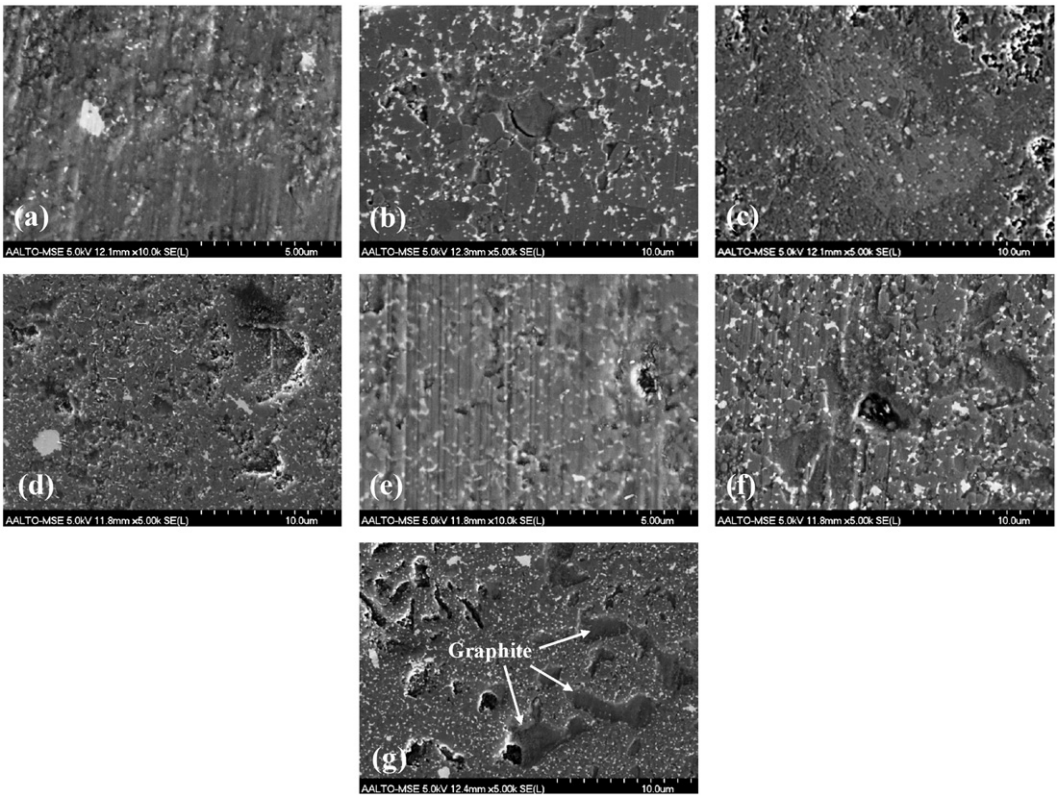

Fig. 10. Worn surfaces of (a) AZ (b) AZCF, (c) AZBF, (d) AZMS, (e) AZWS, (f) AZBN and (g) AZGR.

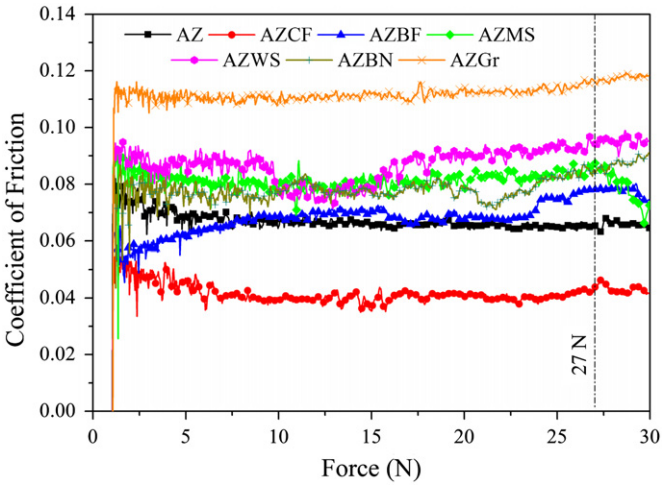

Fig. 11. Representative coefficient of friction curves (out of three for each material) from scratch tests.

alumina even though the grain size of alumina is similar in both composites.

The highest hardness for the composites was obtained with AZMS, but hardness of AZWS and AZCF was also relatively high, although the composites were not fully dense. It was shown previously [42] that similarly to the AZ indentation curves, AZMS showed only minor variation, while for example; in the AZGR indentation curves there was large variation (Fig. 9). When comparing close to fully dense materials AZCF, AZBN, and AZBF, it is clear that BaF_2 and especially h-BN additions decreased more the hardness than CaF_2. Presence of graphite reduced the hardness of the material significantly. The similar hardness values of AZ and pure alumina can be attributed to the addition of nanosized zirconia and relatively small alumina grain size. Suppressed grain growth in AZ and composites had direct influence on the hardness. The sub-micron size grains of alumina and nanosized grains of zirconia, latter ones being located at the Al_2O_3 grain boundaries, together with the fast sintering process has minimized the grain growth of alumina and zirconia during sintering. Differences in densification of the composites also had impact on their mechanical properties. The Young's modulus of AZ was lower than those of the PECSed $Al_2O_3+ZrO_2$ (3 mol% Y_2O_3) [44] and pure alumina [44,45]. It was very similar for all the materials except AZWS and AZGR, which showed relatively poor densification, and had lower modulus. In AZCF the additive particles were strongly bonded with the matrix and as a result its hardness was very close to the matrix. It also had very smooth and almost defect free surface. AZMS had a lower relative density than AZCF but its hardness was higher likely due to the shape of the additive particles, which was also the case for AZWS. In microhardness test it is very probable that the diamond tip is indenting mostly into the matrix and hitting a very small fraction of a MoS_2 or WS_2 particle, because of their needle like shapes. AZGR was not fully dense, and the

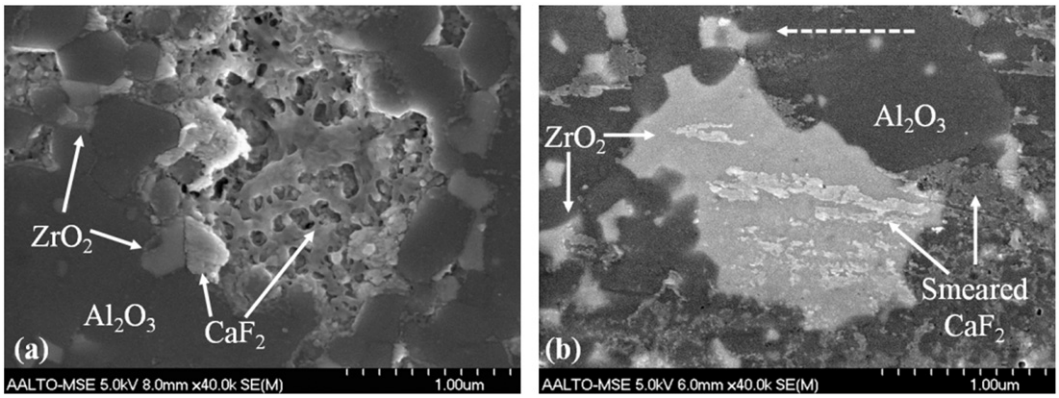

Fig. 12. Microstructure of AZCF. (a) Material removal and displacement around CF grains and (b) smearing of CF onto the ceramic matrix. Dashed arrow indicates the scratch direction.

load applied in the test seemed to be too high for the large graphite flakes and their surrounding nanostructured matrix. Insufficient adhesion and large size of h-BN particles had a negative effect on the hardness of AZBN.

Coefficient of friction of the composites was investigated by two different methods. Scratch test was carried out with dynamic loading using a diamond tip and pin-on-disk test was held under static force and constant distance using an alumina ball. The former was made in order to prevent any influence of a reaction at the contact zone due to the increasing temperature. The diamond stylus has very low friction against smooth surfaces based on its superior hardness and surface properties, which is the reason for very low CoF values compared to pin-on-disk test results.

In scratch tests AZ matrix showed relatively low CoF compared to composites owing to its smooth and intact surface, which was a problem in presence of solid lubricant flakes. During the scratch test the Rockwell diamond tip penetrated under the surface during its linear movement as the applied force increased. It went easily through the soft surface phases, but the ceramic matrix was strong enough to resist the pressure quite well. Therefore, the lamellar and sheet like soft particles broke first and then the matrix at the nearby region failed or fractured. In AZCF the lubricious effect of CaF_2 reduced the CoF by half relative to the other solid lubricants and clearly also when compared to AZ. Material transfer and formation of soft tribo film reduced the CoF significantly even though it was not continuous.

In pin-on-disk tests the measured values correspond well with the results obtained for the alumina–zirconia ceramics at room temperature [51]. Although the CoF of the composites were very similar and relatively high due to the low amounts of low friction additives, there were some changes regarding to the different characteristics of the solid lubricants. MoS_2 and graphite are very effective lubricants at room temperature but they lose their effectiveness at elevated temperatures due to oxidation driven structural degradation. AZWS had almost the same behaviour with AZMS, owing to the similarities between MoS_2 and WS_2. AZCF and AZBF had the same CoF, which is higher than that for AZMS and AZGR. This is consistent with the fact that CaF_2 and BaF_2 usually work better at elevated temperatures ($>500\ ^{\circ}C$) and at room temperature only when incorporated with a soft metal (e.g., Ag) as a result of synergistic effect [22]. Hexagonal boron nitride has a high chemical inertness and its sintering temperature is higher than the processing temperature of AZBN. Higher CoF of AZBN can be attributed to the poor bonding of h-BN particles with the AZ matrix during sintering and removal of additive phase from the surface of the sintered compacts during surface preparation for the pin-on-disk tests. Lack of a continuous and thick enough soft and lubricating film prevented lower friction in all composites. These results are in accordance with the preliminary findings of the authors with the similar composites tested by a reciprocal ball-on-plate tribometer [37]. Addition of the same solid lubricants to AZ matrix in 1 wt% the reduced the CoF from 0.5 to approximately 0.3 at room temperature. CoF was 0.4 in addition of MoS_2 and WS_2, and it was 0.3 when other solid lubricants were used.

Even though AZ had the highest microhardness, it showed the highest wear rate among the materials because of the direct tribo contact between AZ matrix surface and alumina counter material. Heavy smearing of the alumina counter material led to formation of third body alumina particles, which is the cause for increased wear. The brittle fractures at the surface dominate the wear mechanism at the room temperature for AZ. In case of the composites the solid lubricants, despite their low amount, lowered the formation of hard abrasive particles to some extent. Except for AZGR the lower wear rates of the composites with the low-friction additives can be correlated with their hardness. For example, AZCF and AZMS had higher hardness than the other materials and their wear rates were also lower. Despite the low microhardness and relatively lower density, these large flake-like regions of graphite worked as solid lubricant reservoirs and lowered CoF as well as wear. The materials in general, behaved as wear resistant composites rather than low friction materials.

5. Conclusions

Ceramic matrix nanocomposites of Al_2O_3+15 wt% (ZrO_2+3 mol% Y_2O_3) with solid lubricant additives were prepared by PECS applying the same processing parameters (1300 °C, 5 min, 50 MPa). Relative density above 99% was obtained in the alumina–zirconia nanocomposite as well as in the composites with the additions of CaF_2, h-BN, and BaF_2. Composites with MoS_2 and graphite were also nearly as dense ($>98.5\%$T.D.), but the material with the addition of WS_2 showed lower density. In presence of CaF_2 the compacts were almost fully dense (99.9% T.D.). Composition of the soft additives was conserved due to short process time, although partial melting of BaF_2 was observed. Grain growth of alumina in the composites was significantly low while some grain growth was observed for zirconia. Grain sizes were measured to be between 390–525 nm and 94–156 for alumina and zirconia, respectively. Grain growth was relatively less for composites with MoS_2 addition. Hardness and Young's modulus of 20.35 ± 0.5 and 322 ± 10 GPa were achieved for the matrix material. Addition of MoS_2 had almost no effect on these values, however, some deficiency of hardness was observed in presence of other solid lubricants, especially for BaF_2, h-BN and graphite. Young's moduli of the materials were quite similar, except for the composite with WS_2. CoF of Al_2O_3+15 wt% (ZrO_2+3 mol% Y_2O_3) against the alumina ball in the pin-on-disc tests has dropped from 0.50 to level of 0.38 in the presence of solid lubricants. Low amount and sparse distribution of solid lubricants seemingly prevented further decrease of CoF values. Al_2O_3+15 wt% (ZrO_2+3 mol% Y_2O_3)$+3$ wt% MoS_2 and Al_2O_3+15 wt% (ZrO_2+3 mol% Y_2O_3)$+3$ wt% Graphite showed the lowest CoF against alumina ball among composite materials. Wear resistance of the matrix material was increased by a factor of two when modified. At room temperature the addition of graphite had a clear effect on both friction and wear properties, despite the relatively poor mechanical properties. CoF determined in the scratch test was the lowest, 0.043, for the composite with CaF_2 in which the additive smeared at the contact between the surface and the diamond tip. Alumina–zirconia nanoceramic had CoF value of 0.068, while the other materials showed even higher values and graphite addition gave the poorest result. This study showed that at room temperature although low amounts of additives has a limited effect on CoF, wear resistance can be improved by one to three orders of magnitude. Tribological performance of the modified composites depends on the amount of low friction additives, which on the other hand was found to degrade the mechanical properties except for MoS_2. At room temperature, when added in amount of 3 wt%, CaF_2 and MoS_2 are promising candidates as low friction aid for alumina zirconia composites.

Acknowledgements

This work was supported by Tekes and consortium of Finnish companies (NEWCON-HTLF), the Korea Foundation for International Cooperation of Science and Technology (KICOS 2008-0143), as well as the Academy of Finland. Mr. R. Maki is thanked for his help.

References

[1] B. Kerkwijk, M. Garcia, W.E. van Zyl, L. Winnubst, E.J. Mulder, D.J. Schipper, H. Verweij, Friction behaviour of solid oxide lubricants as second phase in α-Al_2O_3 and stabilised ZrO_2 composites, Wear 256 (1–2) (2004) 182–189.

[2] V. Trombini, E.M.J.A. Pallone, U. Anselmi-Tamburini, Z.A. Munir, R. Tomasi, Characterization of alumina matrix nanocomposite with ZrO_2 inclusions densified by spark plasma sintering, Materials Science and Engineering A 501 (1–2) (2009) 26–29.

[3] G.-D. Zhan, J. Kuntz, J. Wan, J. Garay, A.K. Mukherjee, A novel processing route to develop a dense nanocrystalline alumina matrix (<100 nm) nanocomposite material, Journal of the American Ceramic Society 86 (1) (2003) 200–202.

[4] R.R. Menezes, R.H.G.A. Kiminami, Microwave sintering of alumina–zirconia nanocomposites, Journal of Materials Processing Technology 203 (1–3) (2008) 513–517.

[5] R. Román, I. Cañadas, J. Rodríguez, M.T. Hernández, M. González, Solar sintering of alumina ceramics: microstructural development, Solar Energy 82 (10) (2008) 893–902.

[6] Z. Shen, M. Johnsson, Z. Zhao, M. Nygren, Spark plasma sintering of alumina, Journal of the American Ceramic Society 85 (8) (2002) 1921–1927.

[7] Z.A. Munir, D.V. Quach, M. Ohyanagi, Electric current activation of sintering: a review of the pulsed electric current sintering process, Journal of the American Ceramic Society 94 (1) (2011) 1–19.

[8] J. Suffner, D. Wang, H. Hahn, Enhancing superplasticity of ZrO_2 (Y_2O_3)–Al_2O_3 composites prepared by spark plasma sintering of metastable powders, Materials Science and Engineering A 527 (29–30) (2010) 7885–7892.

[9] F. Wakai, Superplasticity of ceramics, Ceramics International 17 (3) (1991) 153–163.

[10] F. Wakai, H. Kato, S. Sakaguchi, N. Murayama, Compressive deformation of Y_2O_3-stabilized ZrO_2/Al_2O_3 composite, International Journal of High Technology Ceramics 3 (3) (1987) 255–255.

[11] F. Wakai, N. Kondo, H. Ogawa, T. Nagano, S. Tsurekawa, Ceramics superplasticity: deformation mechanisms and microstructures, Materials Characterization 37 (5) (1996) 331–341.

[12] K. Morita, K. Hiraga, B.N. Kim, Effect of minor SiO_2 addition on the creep behaviour of superplastic tetragonal ZrO_2, Acta Materials 52 (11) (2004) 3355–3364.

[13] Y. Sakka, T. Ishii, T.S. Suzuki, K. Morita, K. Hiraga, Fabrication of high-strain rate superplastic yttria-doped zirconia polycrystals by adding manganese and aluminum oxides, Journal of the European Ceramic Society 24 (2) (2004) 449–453.

[14] T.S. Suzuki, Y. Sakka, K. Morita, K. Hiraga, Enhanced superplasticity in a alumina-containing zirconia prepared by colloidal processing, Scripta Materialia 43 (8) (2000) 705–710.

[15] D. Sarkar, S. Adak, N.K. Mitra, Preparation and characterization of an Al_2O_3–ZrO_2 nanocomposite, Part I: Powder synthesis and transformation behaviour during fracture, Composites Part A—Applied Science 38 (1) (2007) 124–131.

[16] B. Kerkwijk, A.J.A. Winnubst, H. Verweij, E.J. Mulder, H.S.C. Metselaar, D.J. Schipper, Tribological properties of nanoscale alumina–zirconia composites, Wear 225–229 (Part 2) (1999) 1293–1302.

[17] J. Wang, R. Stevens, Zirconia-toughened alumina (ZTA) ceramics, Journal of Materials Science 24 (10) (1989) 3421–3440.

[18] B. Kerkwijk, L. Winnubst, E.J. Mulder, H. Verweij, Processing of homogeneous zirconia-toughened alumina ceramics with high dry-sliding wear resistance, Journal of the American Ceramic Society 82 (8) (1999) 2087–2093.
[19] A. Skopp, M. Woydt, Ceramic–ceramic composite materials with improved friction and wear properties, Tribology International 25 (1) (1992) 61–70.
[20] T. Murakami, J.H. Ouyang, S. Sasaki, K. Umeda, Y. Yoneyama, High-temperature tribological properties of spark-plasma-sintered Al_2O_3 composites containing barite-type structure sulfates, Tribology International 40 (2) (2007) 246–253.
[21] J.H. Ouyang, S. Sasaki, T. Murakami, K. Umeda, Tribological properties of spark-plasma-sintered $ZrO_2(Y_2O_3)$–CaF_2–Ag composites at elevated temperatures, Wear 258 (9) (2005) 1444–1454.
[22] J.H. Ouyang, Y.F. Li, Y.M. Wang, Y. Zhou, T. Murakami, S. Sasaki, Microstructure and tribological properties of $ZrO_2(Y_2O_3)$ matrix composites doped with different solid lubricants from room temperature to 800 °C, Wear 267 (9–10) (2009) 1353–1360.
[23] J.H. Ouyang, S. Sasaki, T. Murakami, K. Umeda, The synergistic effects of CaF_2 and Au lubricants on tribological properties of spark-plasma-sintered $ZrO_2(Y_2O_3)$ matrix composites, Materials Science and Engineering A 386 (1–2) (2004) 234–243.
[24] J.H. Ouyang, S. Sasaki, T. Murakami, K. Umeda, Spark-plasma-sintered $ZrO_2(Y_2O_3)$–$BaCrO_4$ self-lubricating composites for high temperature tribological applications, Ceramics International 31 (4) (2005) 543–553.
[25] C. Donnet, A. Erdemir, Historical developments and new trends in tribological and solid lubricant coatings, Surface and Coatings Technology 180–181 (2004) 76–84.
[26] A. Erdemir, Review of engineered tribological interfaces for improved boundary lubrication, Tribology International 38 (3) (2005) 249–256.
[27] H.E. Sliney, Solid lubricant materials for high temperatures—a review, Tribology International 15 (5) (1982) 303–315.
[28] S.P. Hannula, E. Turunen, J. Koskinen, O. Söderberg, Processing of hybrid materials for components with improved life-time, Current Applied Physics 9 (3, Supplement 1) (2009) S160–S166.
[29] J.H. Ouyang, S. Sasaki, K. Umeda, The friction and wear characteristics of low-pressure plasma-sprayed ZrO_2–$BaCrO_4$ composite coating at elevated temperatures, Surface and Coatings Technology 154 (2–3) (2002) 131–139.
[30] O. Tingaud, P. Bertrand, G. Bertrand, Microstructure and tribological behaviour of suspension plasma sprayed Al_2O_3 and Al_2O_3–YSZ composite coatings, Surface and Coatings Technology 205 (4) (2010) 1004–1008.
[31] E.D.H. Hübner, Alumina Processing, Properties and Applications, Springer-Verlag, New York, 1984.
[32] P. Rao, M. Iwasa, I. Kondoh, Properties of low-temperature-sintered high purity α-alumina ceramics, Journal of Materials Science Letters 19 (7) (2000) 543–545.
[33] Z. Munir, U. Anselmi-Tamburini, M. Ohyanagi, The effect of electric field and pressure on the synthesis and consolidation of materials: a review of the spark plasma sintering method, Journal of Materials Science 41 (3) (2006) 763–777.
[34] R. Orrù, R. Licheri, A.M. Locci, A. Cincotti, G. Cao, Consolidation/synthesis of materials by electric current activated/assisted sintering, Materials Science and Engineering R 63 (4–6) (2009) 127–287.
[35] C.M. Carney, T.-I. Mah, Current isolation in spark plasma sintering of conductive and nonconductive ceramics, Journal of the American Ceramic Society 91 (10) (2008) 3448–3450.
[36] Y. Zhou, K. Hirao, Y. Yamauchi, S. Kanzaki, Densification and grain growth in pulse electric current sintering of alumina, Journal of the European Ceramic Society 24 (12) (2004) 3465–3470.
[37] S.-H. Kim, S.-H. Cho, S.-P. Hannula, S.W. Lee, Effects of different solid lubricants on mechanical and tribological properties of Al_2O_3/ZrO_2 nanocomposites, Materials Science Forum 658 (2010) 404–407.
[38] K. Vanmeensel, A. Laptev, O. Van der Biest, J. Vleugels, Field assisted sintering of electro-conductive ZrO_2-based composites, Journal of the European Ceramic Society 27 (2–3) (2007) 979–985.
[39] G. Bernard-Granger, C. Guizard, Spark plasma sintering of a commercially available granulated zirconia powder: I. sintering path and hypotheses about the mechanism(s) controlling densification, Acta Materialia 55 (10) (2007) 3493–3504.
[40] S.J. Park, K. Cowan, J.L. Johnson, R.M. German, Grain size measurement methods and models for nanograined WC-Co, International Journal of Refractory Metals and Hard Materials 26 (3) (2008) 152–163.
[41] K. Mannesson, M. Elfwing, A. Kusoffsky, S. Norgren, J. Agren, Analysis of WC grain growth during sintering using electron backscatter diffraction and image analysis, International Journal of Refractory Metals and Hard Materials 26 (5) (2008) 449–455.
[42] M.E. Cura, S.H. Kim, S.H. Cho, T. Suhonen, T. Muukkonen, A. Vaajoki, O. Söderberg, U. Kanerva, S.W. Lee, S.P. Hannula, Pulsed electric current sintering of the Al_2O_3–15 wt% ZrO_2 nanocomposites with 3 wt% of different solid lubricants, Materials Science Forum 695 (2011) 473–476.
[43] I. Levin, D. Brandon, Metastable alumina polymorphs: crystal structures and transition sequences, Journal of the American Ceramic Society 81 (8) (1998) 1995–2012.
[44] W.H. Tuan, S.M. Liu, C.J. Ho, C.S. Lin, T.J. Yang, D.M. Zhang, Z.Y. Fu, J.K. Guo, Preparation of Al_2O_3–ZrO_2–Ni nanocomposite by pulse electric current and pressureless sintering, Journal of the European Ceramic Society 25 (13) (2005) 3125–3133.
[45] S. Huang, K. Vanmeensel, O. Van der Biest, J. Vleugels, Pulsed electric current sintering and characterization of ultrafine Al_2O_3–WC composites, Materials Science Engineering, A 527 (3) (2010) 584–589.
[46] G.-D. Zhan, J. Kuntz, J. Wan, J. Garay, A.K. Mukherjee, Alumina-based nanocomposites consolidated by spark plasma sintering, Scripta Materialia 47 (11) (2002) 737–741.
[47] M.E. Cura, R. Ritasalo, U. Kanerva, J. Syrén, J. Oksanen, J. Lotta, T. Suhonen, J. Lagerbom, O. Söderberg, E. Turunen, S.-P. Hannula, Pulsed electric current sintering of tic- powders and effect of binder content on microstructure and mechanical properties, in: World Powder Metallurgy Congress, Florence, Italy, 2010.
[48] R.H.J. Hannink, P.M. Kelly, B.C. Muddle, Transformation toughening in zirconia-containing ceramics, Journal of the American Ceramic Society 83 (3) (2000) 461–487.
[49] J. Chevalier, L. Gremillard, A.V. Virkar, D.R. Clarke, The tetragonal-monoclinic transformation in zirconia: lessons learned and future trends, Journal of the American Ceramic Society 92 (9) (2009) 1901–1920.
[50] S. Fabris, A.T. Paxton, M.W. Finnis, A stabilization mechanism of zirconia based on oxygen vacancies only, Scripta Materialia 50 (20) (2002) 5171–5178.
[51] K. Miyoshi, S.C. Farmer, A. Sayir, Wear properties of two-phase Al_2O_3/ZrO_2 (Y_2O_3) ceramics at temperatures from 296 to 1073 °C, Tribology International 38 (11–12) (2005) 974–986.